Received: 15 February 2023 | Revised: 26 May 2023 | Accepted: 30 May 2023

DOI: 10.1002/ar.25281

SPECIAL ISSUE ARTICLE

The Anatomical Record WILEY

Uncovering the adult morphology of the forearm bones from the Sima de los Huesos Site in Atapuerca (Spain), with comments on biomechanical features

Laura Rodríguez[1,2] | **Rebeca García-González**[2] | **Juan Luis Arsuaga**[3,4] | **José-Miguel Carretero**[2,3,5]

[1]Departamento de Biodiversidad y Gestión Ambiental, Universidad de León, Facultad de Ciencias Biológicas y Ambientales, León, Spain

[2]Laboratorio de Evolución Humana, Universidad de Burgos, Burgos, Spain

[3]Centro UCM-ISCIII de Investigación sobre Evolución y Comportamiento Humanos, Madrid, Spain

[4]Departamento de Geodinámica, Estratigrafía y Paleontología, Facultad de Ciencias Geológicas, Universidad Complutense de Madrid, Madrid, Spain

[5]Unidad Asociada de I+D+I al CSIC Vidrio y Materiales del Patrimonio Cultural (VIMPAC), Burgos, Spain

Correspondence
Laura Rodríguez, Departamento de Biodiversidad y Gestión Ambiental, Universidad de León, Facultad de Ciencias Biológicas y Ambientales, Campus de Vegazana, Avda. Emilio Hurtado, 24071 León, Spain.
Email: lrodg@unileon.es

Funding information
Fieldwork at the Atapuerca sites is funded by the Junta de Castilla y León and the Fundación Atapuerca; MCIN/AEI/10.13039/501100011033/FEDER, UE, Grant/Award Number: PID2021-122355NB-C31

Abstract

The forearm skeleton is composed of two bones: the radius and the ulna. This is closely related to manipulative movements. The ulna is part of the elbow joint, whereas the radius and ulna together with the scaphoid and lunate bones, form the wrist joints. Thus, morphofunctional analysis of the adult Sima de los Huesos (SH) forearm bones, provides clues about manipulative activities in one Pleistocene population. From 1976 to the present, over 7000 human fossils have been recovered from the SH site. The radial sample comprised 98 labeled fragments, of which 49 belonged to adult individuals, representing at least 7 individuals. The ulnar sample included 31 labeled adult fossils representing at least nine individuals. In this study, we describe the SH radii and ulnae and analyze their functional implications for manipulative and forearm movements. We confirmed that the SH radii are long and curved, with variations in robusticity and radial tuberosity orientation. The SH ulnae are characterized by an anteriorly oriented trochlear notch, a massive olecranon process, an obliquely oriented radial notch, a blunt and short supinator crest, a gracile and curved diaphysis, and a round and anteriorly oriented pronator crests. In general, they exhibit Neanderthal morphology. The SH collection provides a unique opportunity to conduct morphological analyses of these bones in the Middle Pleistocene population.

KEYWORDS

Forearm, Morphological and Biomechanical traits, Radio, Sima de los Huesos, Ulna

1 | INTRODUCTION

The upper extremity is composed of three long bones: the humerus, radius, and ulna, as well as the smaller bones of the hand. It can be analyzed mechanically as an open kinetic chain, with the humerus being the proximal upper limb bone, which articulates with the scapular girdle proximally and the ulna distally at the elbow. The ulna and radius comprise the forearm and are articulated distally with the scaphoid and lunate of the wrist. Because of this medial position in the chain, the forearm is often analyzed for its importance in manipulator behavior (Antón & Polidoro, 2000; Trinkaus & Churchill, 1988). It is well known that the position of some forearm bone traits is related to the loading and lever arm. These two bones are essential for manipulation and their shapes provide valuable information regarding their functional morphologies.

In comparison to modern human morphology, Neanderthals have strongly laterally curved radial shafts, anteroposteriorly expanded radial heads and both absolutely and relatively long necks (Boule, 1911; De Groote, 2011; Trinkaus, 1983; Trinkaus & Churchill, 1988). Neanderthal ulna remains are characterized by a curved diaphysis, with a posterior subtense, anteriorly facing trochlear notch, and a very anteroposterior projected insertion for *m. pronator quadratus* (De Groote, 2011; Pérez-Criado & Rosas, 2017; Trinkaus, 1983; Trinkaus & Churchill, 1988). This morphology is believed to support more powerful pronation-supination and flexion-extension movements. In addition to bone morphology, it is assumed that Neanderthals have powerful forearms because of the well-pronounced muscle attachment sites on their upper limb bones (De Groote, 2011; Trinkaus & Churchill, 1988).

The radial subtense, supinator crest, and position of the radial tuberosity may indicate that Neanderthals closely resemble earlier hominins in terms of morphology and strength of the radius and that the Neanderthal forearm and elbow were especially strong during pronation and supination (De Groote, 2011; Trinkaus & Churchill, 1988). The Neanderthal ulna is defined as a gracile (Trinkaus, 1983), and the proximal ulna is described as having a more anteriorly facing trochlear notch than in modern humans (De Groote, 2011; Trinkaus & Churchill, 1988). The *m. pronator quadratus* crest in Neanderthals is very pronounced, although the interosseous crest is poorly developed as it is on the radius (Aiello & Dean, 1990; De Groote, 2011; Pérez-Criado & Rosas, 2017; Trinkaus & Churchill, 1988).

The Neanderthal body is considered to have a wide trunk and shortened distal limb segments compared to modern archaic humans as an adaptation to cold climates (Trinkaus, 1981). However, other traits, such as nose proportions, morphology, and frontal sinus size, do not seem to support the climate hypothesis (Balzeau et al., 2023; Holton & Franciscus, 2008; Li et al., 2023; Rae et al., 2011), leaving genetic drift as a potential explanation for Neanderthal body shape (Weaver, 2009).

As described previously (Rodríguez et al., 2016), radial remains from the SH have traits that differentiate them from those of recent humans and make them more similar to Neanderthals. In contrast, the SH sample also differs from Neanderthals in showing high overall gracility, as well as a high frequency (80%) of anteriorly oriented radial tuberosity and thick cortices (Rodríguez et al., 2016). The characteristics of the SH ulnae were only sketched in Arsuaga et al. (2015).

Thus, this study had two aims. First, to update the radial remains from an earlier description (Rodríguez et al., 2016) and second, to introduce the ulna remains recovered from the Sima de los Huesos (SH) site in Sierra de Atapuerca from 1976 to the present. These fossils have been dated to more than 430 ky (thousands of years ago). This study also contributes to the creation of an illustrated catalog from the SH to aid in the comparison of these specimens with others in paleoanthropological contexts. Finally, this paper presents analyses of bones relative to their morphofunctional roles and biomechanics.

2 | MATERIALS AND METHODS

2.1 | SH sample

Since 1976 over 7000 human fossils have been recovered from the SH site, of which 458 represent arm bones. The radial sample consisted of 49 labeled adult specimens. Regarding the ulnae, there were 31 labeled adult fossils. In this study, only significant elements are discussed.

We provide detailed photographs of the bones and their features based on the original SH specimens. We did not report detailed anatomical descriptions of every specimen, and only the main anatomical features were highlighted based on adult specimens. We also reported an inventory of the most complete specimens and basic measurements obtained using standard anthropological techniques (Martin & Saller, 1957). All labeled fragments were named AT (i.e., Atapuerca and SH), followed by Arabic numbers (for example, AT-251). We give a bone abbreviation, represented by "R" for the radius and "UL" for the ulna only when the proximal half of the bone is present.

Some of these radii have been published previously (Rodríguez et al., 2016). Here, we update the inventory and summarize the biomechanical implications of their morphology. The SH ulnar remains are unpublished, although some traits have been described by (Arsuaga et al., 2015).

2.2 | Radial SH Inventory and minimum number of individuals (MNI)

To date, there have been 49 labeled adult radial fragments, which comprise a minimum of 12 adult elements (Table 1) and represent 7 adult individuals. The SH radii were published by Rodríguez et al. (2016). Table 2 contains only some of the main dimensions for characterizing the radial traits in the most complete adult specimens. Table 3 lists the basic statistics of the SH specimens. Rodríguez et al. (2016) presented statistical comparisons of Neanderthal and modern human samples, although specific comparisons for these particular measurements are also shown in Table 2. Figure 1 shows the most complete radial remains of the SH sample. In Figures 2–9, we present anatomical views of these complete specimens.

TABLE 1 Adult radial inventory at Sima de los Huesos (SH).

Label	Side	Description
R-I	Right	Complete
R-II	Left	Complete
R-III	Right	Proximal one-third fragment
R-IV	Left	Complete
R-V	Right	Complete
R-VI	Right	Complete
R-VII	Right	Complete
R-IX	Left	Proximal two-thirds fragment
R-X	Left	Complete
R-XI	Left	Complete
R-XIV	Left	Proximal one-third fragment
R-XV	Right	Proximal three-fourths fragment

Note: R-I = AT-795+1097+1118.
R-II = AT-1090+1091+1092.
R-III = AT-1260.
R-IV = AT-2474+2493.
R-V = AT-2498+2961+2960+3279.
R-VI = AT-2483+2488+2575+3277.
R-VII = AT-3281+3282.
R-IX = AT-2953+2959.
R-X = AT-1087+1109+2864.
R-XI = AT-1782+2032.
R-XIV = AT-1702.
R-XV = AT-6184+5625+5641.

2.3 | Ulnar SH Inventory and MNI

The sample comprised 31 adult label fragments assembled into 16 elements representing at least nine adult individuals. Table 4 contains the inventory of all ulnar specimens ordered by ulna number and a brief description. Tables 5 and 6 list the main dimensions, basic statistics, and comparison of the most complete specimens. In Figure 10, we show the most complete ulnar remains from the SH sample, and in Figures 11–19, we present anatomical views of the most complete specimens.

2.4 | Comparative sample

For comparative purposes, we also studied the following Pleistocene fossil specimens: the originals of La Ferrassie 1 and 2, La Chapelle-aux-Saints 1 (Musée de l'Homme, Paris), and the casts of Spy 1, Neanderthal 1, and Tabun

TABLE 2 Radial measurements for adult specimens at Sima de los Huesos (SH).

Side	RI Right	RII Left	RIV Left	RV Right	RVI Right	RVII Right	RX Left	RXI Left	R-XIV Left	R-XV Right
Maximum length (M1)	222.0	241.0	255.0	256.0	243.0	253.0	221.0	249.0		
Head AP diameter (M-5.1)	20.0	23.5	22.7	24.0	20.4	22.3	18.9	21.1	*19.5	22.2
Head ML diameter (M-4.1)	18.8	22.9	21.1	23.7	20.7	21.0	18.1	*19.9	*18.7	21.6
Fischer Neck length (FNL)	23.8	25.8	28.3	27.1	24.0	30.6	24.0	30.3	22.0	23.4
Interosseous ML diameter (M-4)	12.6	14.9	14.4	17.8	16.5	14.2	12.6	13.4		17.2
Interosseous AP diameter (M-5)	9.9	12.3	*12.4	12.9	12.8	13.9	9.6	12.3		10.3
Distal epiphyseal breadth (M-5.6)	30.0	34.0	37.0	36.0	37.0	32.0	28.0	33.0		
Diaphysis subtense (M-6)	5.5	4.7	8.5	8.4	6.1	9.6	6.8	8.9		
Diaphysis chord (M-6.1)	157.0	160.0	191.5	200.3	169.7	184.5	160.4	177.9		
Neck angle (M-7)	165.0	171.0	171.0	169.0	166.0	165.0	168.0	165.0	166.0	166.0

*Estimated value.
Note: Linear measurements in mm. Neck angles in degrees.
M: Martin & Saller, 1957.
T: Trinkaus, 1983.

TABLE 3 Main basic statistics, normality test and comparison of radii at Sima de los Huesos (SH). Measurements in millimeters.

					Normality		Variances		ANOVA/ Kruskal–Wallis		Post-hoc: Bonferroni/U-Mann–Whitney		
		Valid	Mean	SD	S-W	*p*-value	Levene	*p*-value	F/ KW	*p*-value	SH- *Homo sapiens*	SH- Neanderthals	Neanderthals- *H. sapiens*
Maximum length (M1)	*H. sapiens*	456	226.13	16.29	1.00	0.207	0.6	0.549	5.13	<0.01	0.015	0.618	0.356
	SH	8	242.50	14.02	0.84	0.081							
	Neanderthals	13	233.27	14.75	0.97	0.83							
Head AP diameter (M-5.1)	*H. sapiens*	388	20.55	2.00	0.99	<0.01			2.66	0.264			
	SH	10	21.36	1.70	0.96	0.767							
	Neanderthals	12	21.35	2.43	0.96	0.811							
Head ML diameter (M-4.1)	*H. sapiens*	388	20.49	2.00	0.99	<0.01			0.45	0.797			
	SH	10	20.67	1.69	0.96	0.74							
	Neanderthals	12	20.15	1.94	0.95	0.634							
Fischer Neck length (FNL)	*H. sapiens*	458	21.09	2.53	0.99	<0.01			18.78	<0.01	<0.01	0.347	0.135
	SH	10	25.71	3.24	0.92	0.389							
	Neanderthals	4	22.63	1.25	0.98	0.911							
Interosseous ML diameter (M-4)	*H. sapiens*	464	15.66	1.78	0.99	<0.001			1.95	0.378			
	SH	9	16.32	1.92	0.82	0.035							
	Neanderthals	8	15.99	1.95	0.95	0.737							
Interosseous AP diameter (M-5)	*H. sapiens*	464	10.92	1.27	0.98	<0.01			5.47	0.065			
	SH	9	11.88	1.44	0.87	0.127							
	Neanderthals	8	10.56	1.49	0.85	0.091							
Distal epiphyseal breadth (M-5.6)	*H. sapiens*	450	31.61	2.99	0.98	<0.01			3.32	0.19			
	SH	8	33.13	3.48	0.91	0.324							
	Neanderthals	5	33.34	2.91	0.78	0.05							
Diaphysis subtense (M-6)	*H. sapiens*	462	5.32	1.24	0.98	<0.01			17.05	<0.01	<0.01	0.592	<0.01
	SH	8	7.24	1.87	0.92	0.398							
	Neanderthals	5	8.30	2.36	0.99	0.965							
Diaphysis chord (M-6.1)	*H. sapiens*	462	168.04	13.36	1.00	0.409			1.41	0.494			
	SH	8	175.16	16.04	0.93	0.482							
	Neanderthals	5	170.20	12.87	0.86	0.240							

TABLE 3 (Continued)

					Normality		Variances		ANOVA/ Kruskal–Wallis		Post-hoc: Bonferroni/U-Mann–Whitney		
		Valid	Mean	SD	S-W	*p*-value	Levene	*p*-value	F/ KW	*p*-value	SH-*Homo sapiens*	SH-Neanderthals	Neanderthals-*H. sapiens*
Neck angle (M-7)	*H. sapiens*	462	169.71	3.33	0.98	<0.01							
	SH	10	167.20	2.39	0.82	<0.01			14.29	<0.01	0.012	0.727	<0.01
	Neanderthals	9	166.78	2.28	0.77	<0.01							

Note: S-W Normality analysis: Shapiro–Wilk test.
Variance Homogeneity test: Levene test.
F/KW: in case of normality and variance homogeneity F-statistic and ANOVA *p*-value are shown in case of normality fail KW-statistic and Kruskal–Wallis *p*-value are presented.
Post hoc analysis: For ANOVA Bonferroni test and for Kruskal–Wallis, U-Mann–Whitney.
Linear measurements in mm. Neck angles in degrees.
Neanderthal sample is composed by La Ferrassie 1 and 2, and La Chapelle-aux-Saints 1, Spy1, Neanderthal 1 and Tabun C1 (originals and cast in the Musée de l'Homme de Paris). Amud 1 (McCown & Keith, 1939), Kebara 2 (Bar Yosef & Vandermeersch, 1991), Shanidar radii (Trinkaus, 1983).

C1, also housed in the Musée de l'Homme de Paris. For the other fossils, we derived data from various bibliographic sources: Amud 1 (McCown & Keith, 1939), Kebara 2 (Bar Yosef & Vandermeersch, 1991), Shanidar radii and ulna (Trinkaus, 1983), Sidron (Pérez-Criado & Rosas, 2017), and Chagyrskaya (Mednikova, 2013).

In addition to the fossils listed above, we jointly studied several modern human samples and named them *Homo sapiens* samples. This modern sample is composed of the "Portuguese sample," which was drawn from individuals belonging to the collections housed in the Bocage Museum (National Museum of Natural History, Lisbon, Portugal) and the Department of Life Sciences at Coimbra University (Coimbra, Portugal). Both collections come from modern cemeteries and are composed of Portuguese people who lived in the nineteenth and twentieth centuries, representing the middle-to-low social class in the cities of Lisbon and Coimbra (Cardoso, 2006; Coqueugniot & Weaver, 2007). The second comparative sample comprised individuals from the Hamann-Todd collection (HTH) housed in the Cleveland Museum of Natural History in Ohio (USA). This sample was divided into two subsamples based on whether they were of African-American or European ancestry. The third sample consisted of individuals from the archeological collection of San Pablo (Burgos), housed in the Laboratory of Human Evolution (Universidad de Burgos, Burgos, Spain). In the third sample, sex was estimated based on non-metric traits of the skull and pelvis using the standards described by (Buikstra & Ubelaker, 1994; Phenice, 1969).

2.5 | Measurements

We provide the basic measurements for both radial and ulnar remains, following Martin and Saller (1957); McHenry et al. (1976); Senut (1980); Solan and Day (1992); Carretero, (1994); Trinkaus, (1983). To take all measurements of the SH specimens and comparative samples, we used standard anthropological techniques and instruments (Mitutoyo digital calipers and osteometry boards for linear measurements). The radial and ulnar curvatures were digitally measured. To this end, we took photographs of the radii and ulnar specimens from the anterior and interosseous views. We outlined each of these photographs using the AUTOCAD software. With these outlines, we established a midline axis, and then calculated the radial curvature as described by Rodríguez et al. (2016), following the instructions of Martin and Saller (1957) and Maia Nieto (1957) (Figure 20a). The ulnar curvature angle was measured as the angle between the proximal and distal parts of the ulnar diaphysis in the

FIGURE 1 Complete radius of Sima de los Huesos Site.

FIGURE 2 Radius I, Right. Scale bar 5 cm. A anterior, M medial, P posterior, L lateral, P Proximal, and D distal views.

FIGURE 3 Radius II, Left. Scale bar 5 cm. A anterior, M medial, P posterior, L lateral, P Proximal, and D distal views.

interosseous view (Figure 20d). The radial tuberosity orientation was calculated as described by Rodríguez et al. (2016) and Maia Nieto (1957) (Figure 20b). The ulnar tuberosity, which is the site of insertion for *m. brachialis*, was also measured in the anterior view with the trochlea positioned anteriorly. The proximal shaft axis was drawn

FIGURE 4 Radius IV, Left. Scale bar 5 cm. A anterior, M medial, P posterior, L lateral, P Proximal, and D distal views.

FIGURE 5 Radius V, Right. Scale bar 5 cm. A anterior, M medial, P posterior, L lateral, P Proximal, and D distal views.

distal to the ulnar tuberosity. We established three different conditions for the ulnar tuberosity (Figure 20c): the proximal axis passed through the central part of the ulnar tuberosity, the proximal axis passed medially through the tuberosity, and the proximal axis did not pass through the ulnar tuberosity. Basic Statistical analyses and comparisons among species were performed using the SPSS v. 26 software (Meulam & Heiser, 2019). We performed the Shapiro–Wilk test to test each sample's normality, followed by the Levene test for testing variance homogeneity. ANOVA and post-hoc analysis were performed when needed. In case of normality or variance homogeneity failure, the Kruskal-Wallis test was performed, followed by post-hoc analysis when required.

3 | RESULTS

3.1 | Radial anatomical clues

Table 7 shows some of the most common radial traits described in the literature for different hominin species and the character states of these traits for the SH radii.

In the next set of figures (Figures 21 and 22), the morphological features of the radius are indicated by capital letters ranging from A to F. Metrically, SH radii are longer bones with longer necks (Figure 21a), lower neck angles (Figure 21b), and greater curvatures (Figure 21c) than those of modern humans, but are similar to those of Neanderthals (Rodríguez et al., 2016). As a consequence of its length, the SH radial diaphysis is, as in some Neanderthals and *Homo antecessor*, gracile (slender) compared with fossil and recent humans (Rodríguez et al., 2016), although no statistical difference in robusticity was found between our modern human sample and the SH.

Although not constant (Figure 21a), the SH radii have relatively longer necks (measured as the distance between radial tuberosity and radial head) than those of recent humans with the same radial articular length (SH Fisher neck index:11.5 ± 0.8 and RH Fisher neck index: 10.0 ± 0.9), as was shown in Rodríguez et al. (2016). The same is true for the Neanderthals and *Homo*

FIGURE 6 Radius VI. Scale bar 5 cm. A anterior, M medial, P posterior, L lateral, P Proximal, and D distal views.

FIGURE 7 Radius VII, Right. Scale bar 5 cm. A anterior, M medial, P posterior, L lateral, P Proximal, and D distal views.

antecessor (De Groote, 2011; Trinkaus, 1983). In addition, although variable, the SH radii share the pattern of a lower neck angle (Table 3) with Neanderthals and are different from those of modern humans, and the curvature index of the SH radii varies from mildly to very curved diaphyses (Rodríguez et al., 2016). Specimens with more anteriorly positioned radial tuberosities and shorter necks (Figure 21a and Figure 22f) tended to be less curved, while specimens that were more curved typically had longer necks (Figure 21) and more medially oriented radial tuberosities (Figure 22f).

On average, the SH radii have an interosseous crest that projects only moderately (Figure 21d) compared to those of recent humans. This trait is shared by the Neanderthals, the Middle Stone Age radius from the Cave of Hearths (Pearson & Grine, 1997), and *H. antecessor* (Carretero et al., 1999).

The main difference between the SH radial remains and Neanderthals was the position of the radial tuberosity (Figure 22f). In the SH samples, 80% of the specimens had a more anterior orientation, similar to that of modern humans, and only two specimens had a medially oriented tuberosity, as in Neanderthals. A medially positioned radial tuberosity is also found in the early hominin specimens AL 288-1p (*Australopithecus afarensis*) and KNM-ER 1500E (*Paranthropus boisei*), as well as the OH 62 (*Homo habilis*) individual and at least one African Pleistocene site (Klasies River). The Lower Pleistocene radius from Gran Dolina-TD6 (*H. antecessor*) showed an anteromedial radial tuberosity similar to that of recent humans (Carretero et al., 1999).

Regarding the radial head (Figure 23), there were no significant differences in anteroposterior (AP) and mediolateral (ML) diameters between groups. Nevertheless, the AP diameter of the radial head in SH is slightly larger than that in ML and similar to that in Neanderthals (De Groote, 2011) but different from that in modern humans.

Regarding the shape of the distal epiphyses (Figure 24), no significant differences were found between the samples (recent humans, SH, and Neanderthals) in distal epiphyseal breadths, either absolutely or relative to the maximum

FIGURE 8 Radius X, Left. Scale bar 5 cm. A anterior, M medial, P posterior, L lateral, P Proximal, and D distal views.

FIGURE 9 Radius XI, Right. Scale bar 5 cm. A anterior, M medial, P posterior, L lateral, P Proximal, and D distal views.

TABLE 4 Adult ulnar inventory at Sima de los Huesos (SH).

Label	Side	Description
UL-I	Right	Proximal three-fourths
UL-II	Right	Distal three-fourths fragment
UL-VI	Left	Proximal two-thirds fragment
UL-VII	Right	Complete
UL-VIII	Left	Complete except styloid process
UL-IX	Left	Proximal two-thirds fragment
UL-X	Right	Proximal three-fourths fragment
UL-XII	Right	Complete except distal epiphysis
UL- XIII	Left	Proximal two-thirds fragment
UL-XIV	Left	Proximal one-half fragment
UL-XV	Left	Olecranon fragment
UL-XVI	Right	Proximal three-fourths fragment
UL-XVIII	Left	Proximal half fragment
UL-XIX	Left	Proximal three-fourths fragment
UL-XXI	Right	Olecranon fragment
UL-XXIII	Left	Proximal one-third fragment

Note: UL-I = AT-669+796.
UL-II = AT-248+1266+1267.
UL-VI = AT-1675+1788.
UL-VII = AT-1105+2480 (Figure 12).
UL-VIII = AT-662+3286 (Figure 13).
UL-IX = AT-1099+2573.
UL-X = AT-1120+2559+2560 (Figure 14).
UL-XII = AT-2962+3863 (Figure 15).
UL- XIII = AT-3284+4022.
UL-XIV = AT-4171+4172.
UL-XV = AT-254.
UL-XVI = AT-488+5791.
UL-XVIII = AT-1104.
UL-XIX = AT-1270.
UL-XXI = AT-2234.
UL-XXIII = AT-5001+5002.

length. Nevertheless, the SH radii had a small styloid process that was directed medially, similar to that in the Neanderthals (Figure 20e). The distal epiphysis of the SH radii is compressed in the AP direction (Figure 21h) compared to both fossil and recent *H. sapiens* (Rodríguez et al., 2016), which is probably related to the anteroposteriorly compressed morphology of the bones of the first carpal row, in the SH hominins (Lorenzo, 2007).

3.2 | Ulnae anatomical clues

Table 8 and Figure 25 show some of the most widely discussed ulnar traits collected in the literature for different hominin species and the characterization of these traits for the SH radial collection. Here, we explain some of them and emphasize the others.

TABLE 5 Adult ulna measurements at Sima de los Huesos (SH).

	UL- I Right	UL-VI Left	UL-VII Right	UL-VIII Left	UL-IX Left	UL-X Right	UL-XII Right	UL-XIII Left	UL-XIV Left	UL-XVI Right	UL-XVIII Left	UL-XIX Left	UL- XXIII Left
Maximum Length (M1)			275	244*			**256***						
Physiological Length (M2)			232	212			**224***						
Trochlear aperture (McH 10)	21.7	17.5		21.0	24.0*		21.1*	18.0	20.9		21.1	18.6	21.7*
Olecranon ML diameter (McH 9)	26.1*	22.6	30.0*	23.7	28.0	27.0	26.0	26.1	28.0		30.2		23.9
Olecranon height (McH 12)	22.2	21.2	25.0	22.6	26.5	24.3	23.9	22.2	23.5		24.8		23.1
Radial notch length (S13)	10.5	11.5	15.6	13	17.4	16.3	14	16.2	16.8	17.1	15.6	12.8	15
Radial notch height (C18)	8	11.9	14.6	11.4	10	12.1	13	12.7	15	13.1	12.3	9.7	11.4
Radial notch position (S&D, 16)	40.3	39.9	49.3	40	44.3	47.2	45.5	39.9	48.2	44.1	44.5		41
Interossoeus crest development (a)	0.2	0.5	1.5	0.3	0.4	0.5	−0.5	−0.8	0.3		−1.5	−0.5	
Proximal AP diameter (McH 13)	17.6	15.5	18.5	13.6	17.5	18.7	16.5	16.9	17.5	17.2	18.3	16	14.9
Proximal ML diameter (McH 14)	15.5	13.4	15	12.2	14.2	15.7	15.1	14.6	13.9	16.6	14.6	13.1	11.9
Subsigmoid AP diameter (M14)	20.6	17.6	23	17.4	23.3	22.7	20	20.2	21.3	21	21.6		19.6
Subsigmoid ML diameter (M13)	18	14.5	25	16	20.3	22.9	20.2	20.4	21.4	21.2	21.1		16.4
Pronator quadratus maximum diameter (T)	14		15.2	9.9		14.3		12.7				12	
Pronator quadratus minimum diameter (T)			10.9	7.9								9	
Pronator perimeter (T)	40		45	31		40		39				37	
Midshaft perimeter (K)	45	38	49	34	45	45	41	45	47		47	47	
Subsigmoid perimeter (T)	62	61	78	51	63	73	67	68	70	67	73		57
Minimum perimeter (T)			38	32			37						
Distal epiphysis maximum diameter (McH 3)			16.0	13.3									
Diaphyseal angle: Curvature	169	173	167	168	167	171	172	168			168	166	

*Estimated measurements. Linear measurements in mm. Neck angles in degrees. (a) Interosseus crest development, calculated as Midshaft ML diameter, Midshaft AP diameter; M, Martin & Saller, 1957; McH, McHenry et al., 1976; S, Senut, 1980; S&D—Solan & Day, 1992; C, Carretero, 1994; T, Trinkaus, 1983. Radial notch Height: Measure as, Maximum length between proximal and distal borders of the radial notch.

TABLE 6 Main basic statistics, normality test, and comparison of ulnae at Sima de los Huesos (SH). Measurements in millimeters.

					Normality		Variances		ANOVA/ Kruskal–Wallis		Post-hoc: Bonferroni/U-Mann–Whitney		
		Valid	Mean	SD	S-W	*p*-value	Levene	*p*-value	F/ KW	*p*-value	SH-*H. sapiens*	SH-Neanderthals	Neanderthals-H. sapiens
Maximum Length (M1)	*H. sapiens*	332	247.29	21.06	0.993	0.150	0.49	0.614	2.366	0.095			
	SH	3	258.33	15.63	0.983	0.752							
	Neanderthals	10	260.65	16.35	0.854	0.065							
Physiological Length (M2)	*H. sapiens*	350	215.53	18.36	0.989	0.012			3.644	0.162			
	SH	3	222.67	10.07	0.987	0.780							
	Neanderthals	6	227.42	14.25	0.921	0.514							
Trochlear aperture (McH 10)	*H. sapiens*	351	23.17	2.42	0.978	<0.01			10.747	<0.01	<0.01	<0.01	0.38
	SH	10	20.56	1.97	0.906	0.258							
	Neanderthals	11	23.72	3.19	0.942	0.547							
Olecranon ML diameter (C6a)	*H. sapiens*	346	23.54	3.27	0.993	0.142	0.83	0.439	11.19	<0.01	<0.01	ns	<0.01
	SH	11	26.51	2.47	0.951	0.656							
	Neanderthals	11	26.63	3.61	0.958	0.741							
Olecranon height (McH 12)	*H. sapiens*	232	20.99	2.83	0.982	<0.01			19.718	<0.01	0.001	0.653	<0.01
	SH	11	23.57	1.53	0.981	0.972							
	Neanderthals	13	24.09	3.65	0.901	0.137							
Radial notch length (S13)	*H. sapiens*	347	17.67	2.83	0.959	<0.01			54.267	<0.01	<0.01	0.068	<0.01
	SH	13	14.75	2.21	0.922	0.263							
	Neanderthals	17	11.38	2.08	0.971	0.842							
Radial notch height (C6a)	*H. sapiens*	347	11.72	2.44	0.764	<0.01			0.618	0.432			
	SH	13	11.94	1.93	0.968	0.869							
	Neanderthals	0											
Radial notch position (S&D, 16)	*H. sapiens*	222	39.06	3.86	0.986	0.032			24.11	<0.01	<0.01	0.451	<0.01
	SH	12	43.68	3.43	0.891	0.122							
	Neanderthals	5	45.48	1.39	0.831	0.141							
Interosseous crest development (a)	*H. sapiens*	350	2.97	1.89	0.885	<0.01			34.415	<0.01	<0.01	0.116	<0.01
	SH	11	0.04	0.81	0.94	0.521							
	Neanderthals	19	0.53	2.76	0.915	0.092							

(Continues)

TABLE 6 (Continued)

					Normality		Variances		ANOVA/ Kruskal–Wallis		Post-hoc: Bonferroni/U-Mann–Whitney		
		Valid	Mean	SD	S-W	*p*-value	Levene	*p*-value	F/ KW	*p*-value	SH-*H. sapiens*	SH-Neanderthals	Neanderthals-H. sapiens
Proximal ML diameter (McH 14)	*H. sapiens*	349	16.63	2.76	0.993	0.131	5.2	0.006	0.206	0.902			
	SH	13	16.82	1.50	0.94	0.462							
	Neanderthals	8	16.68	1.43	0.915	0.389							
Proximal AP diameter (McH 13)	*H. sapiens*	350	15.57	2.06	0.987	<0.01			10.137	0.006	0.024	< 0.01	0.029
	SH	13	14.29	1.37	0.975	0.949							
	Neanderthals	8	17.38	2.29	0.925	0.474							
Subsigmoid ML diameter (M13)	*H. sapiens*	350	21.63	3.39	0.995	0.251	2.90	0.056	0.475	0.622			
	SH	12	20.69	1.90	0.942	0.525							
	Neanderthals	18	20.51	3.05	0.978	0.924							
Subsigmoid AP diameter (M14)	*H. sapiens*	350	20.10	2.63	0.989	0.013			1.147	0.564			
	SH	12	19.78	3.03	0.953	0.685							
	Neanderthals	19	20.64	2.69	0.945	0.319							
Pronator quadratus maximum diameter (T)	*H. sapiens*	350	12.14	1.60	0.994	0.201	0.23	0.795	0.997	0.37			
	SH	6	13.02	1.91	0.953	0.765							
	Neanderthals	3	12.63	2.03	0.83	0.188							
Pronator quadratus minimum diameter (T)	*H. sapiens*	350	10.31	1.36	0.978	<0.01			5.858	0.053			
	SH	3	9.27	1.52	0.977	0.708							
	Neanderthals	3	8.77	0.71	0.974	0.688							
Distal epiphysis maximum diameter (McH 3)	*H. sapiens*	332	16.41	2.30	0.994	0.181	0.888	0.412	0.712	0.492			
	SH	2	14.65	1.91									
	Neanderthals	11	16.75	1.68	0.973	0.918							
Pronator perimeter (T)	*H. sapiens*	343	37.48	4.66	0.946	<0.01			2.483	0.289			
	SH	6	38.67	4.59	0.936	0.631							
	Neanderthals	3	33.77	4.13	0.781	0.069							
Midshaft perimeter (K)	*H. sapiens*	342	44.55	5.39	0.984	<0.01			5.89	0.053			
	SH	11	43.91	4.48	0.845	0.036							
	Neanderthals	4	38.00	2.94	0.882	0.348							

TABLE 6 (Continued)

					Normality		Variances		ANOVA/ Kruskal–Wallis		Post-hoc: Bonferroni/U-Mann–Whitney		
		Valid	Mean	SD	S-W	*p*-value	Levene	*p*-value	F/ KW	*p*-value	SH-*H. sapiens*	SH-Neanderthals	Neanderthals-*H. sapiens*
Subsigmoid perimeter (T)	*H. sapiens*	343	67.19	8.01	0.986	<0.01			0.237	0.626			
	SH	12	65.83	7.51	0.981	0.986							
	Neanderthals	0											
Curvature	*H. sapiens*	84	174.73	3.36	0.94	<0.01							
	SH	10	168.90	2.33	0.90	0.230			25.733	<0.01	<0.01	0.325	<0.01
	Neanderthals	7	171.14	2.12	0.85	0.854							

Note: S-W Normality analysis: Shapiro–Wilk test.
Variance Homogeneity test: Levene Test.
F/KW: in case of normality and variance homogeneity F-statistic and ANOVA *p*-value are shown in case of normality fail KW-statistic and Kruskal-Wallis *p*-value are presented.
Post hoc analysis: For ANOVA Bonferroni test and for Kruskal–Wallis, U-Mann–Whitney.
Neanderthal sample: La Ferrassie 1 and 2, and La Chapelle-aux-Saints 1, Spy1, Neanderthal 1 and Tabun C1 (originals and cast in the Musée de l'Homme de Paris). Amud 1 (McCown & Keith, 1939), Kebara 2 (Bar Yosef & Vandermeersch, 1991), Shanidar radii and ulna (Trinkaus, 1983), Sidron (Pérez-Criado & Rosas, 2017), and Chagyrskaya (Mednikova, 2013).

The SH ulna remains had a high and massive olecranon process (Figure 25a), which was square-shaped when observed in the proximal view (Figure 25l). The SH ulnae were oriented anterior to the trochlear notch (Figure 25k).

Regarding the diaphysis, the SH ulna had a high curvature in the interosseous view (Figure 20 for measurement description and Figure 25c). This feature is similar to that of the Neanderthals (De Groote, 2011; Pérez-Criado & Rosas, 2017 and references therein). In addition, the *m. brachialis* insertion (Figure 25b) is located medially and more distally than in modern humans, and *m. pronator quadratus* insertion (Figure 25d) is projected anteriorly, as in Neanderthals (Arsuaga et al., 2015; De Groote, 2011; Pérez-Criado & Rosas, 2017 and references therein). Similar to the radius, the ulnae have a weak interosseous crest (Figure 25e), similar to those of Neanderthals and the Omo L40-19 ulna (*Paranthropus aethiopicus*, Aiello et al., 1999), and thus a more rounded diaphysis than that of modern humans (Aiello & Dean, 1990; Arsuaga et al., 2015). They also had thick cortices on their diaphyses (Figure 25n).

Proximally, they had a rounded and well-developed supinator crest (Figure 25f), as was witnessed in Neanderthals (Arsuaga et al., 2015). This feature is related to the position of the radial facet (Figure 25g), which arises from the diaphysis and is obliquely displaced forward. Additionally, the radial facet has a teardrop or trapezoidal shape, being more super inferiorly elongated than modern humans, more horizontally rectangular, and similar to the Sidrón Neanderthals (Arsuaga et al., 2015; Pérez-Criado & Rosas, 2017).

In the lateral or medial view, the diaphysis is curved in the anteroposterior direction. The posterior border is straight in its distal two-thirds but slopes anteriorly in its proximal third (Figure 25i), displacing the olecranon and trochlear process anteriorly (Figure 25h), as in the Omo L40-19 (*Paranthropus aethiopicus*, Aiello et al., 1999) and Neanderthal ulnae (Aiello & Dean, 1990; McHenry et al., 1976).

SH bones generally had thick cortices (Figure 25n). Few studies have analyzed the ulnar bone thickness (Trinkaus et al., 1999). The mean cortical thickness of the left ulnar SH (%CA = 87 ± 0.4, $n = 4$) was similar to that of the Saint-Césaire left ulna (%CA = 89).

Finally, the ulnar head, although variable (Figure 25m1 and m2), is typically anteroposteriorly elongated relative to modern humans and has a small styloid process (Figure 25j).

4 | DISCUSSION

The Neanderthal pattern for the radii, with a long radial neck with a low neck angle, the more medial orientation

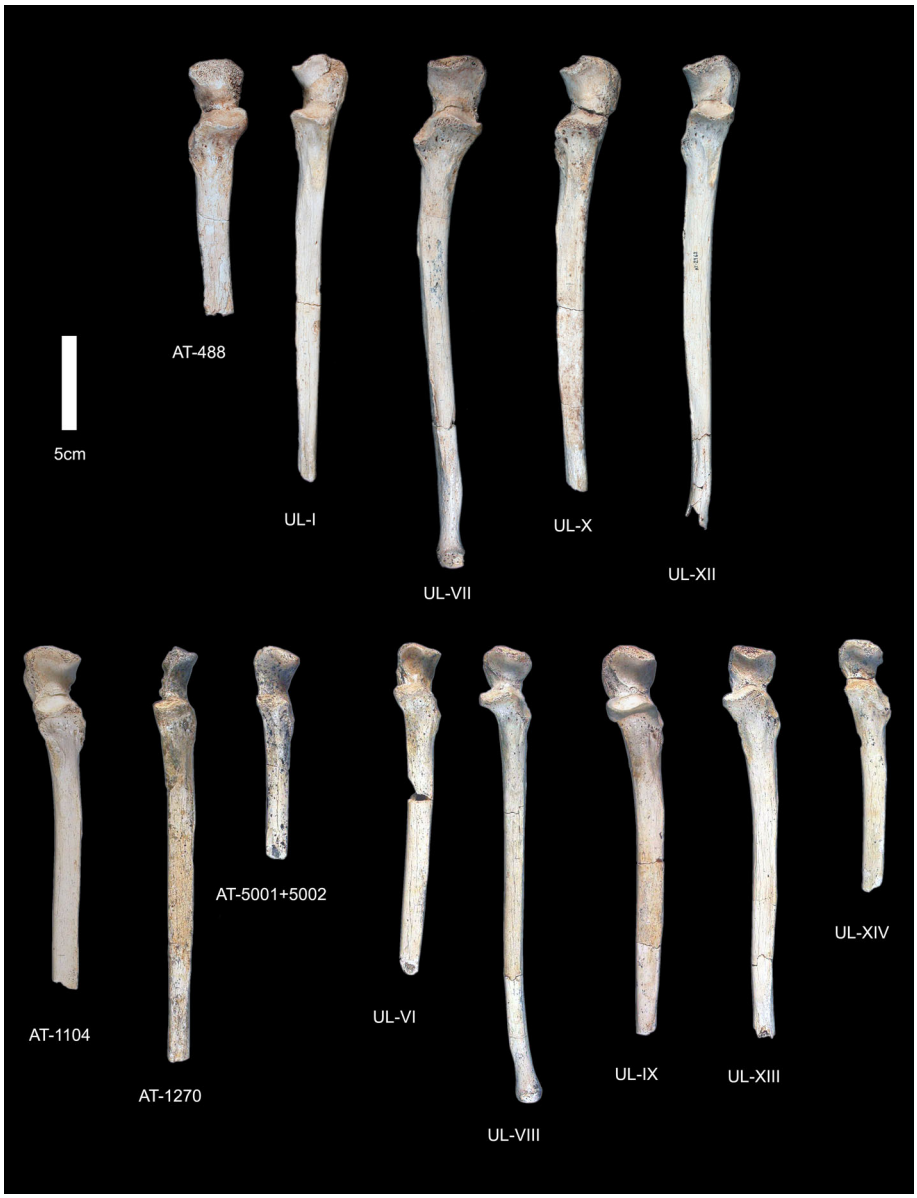

FIGURE 10 Most representative Sima de los Huesos ulnar fragments.

of the radial tuberosity, and high shaft curvature, is consistent with very powerful forearms and pronation/supination movements that provide manipulation and other mechanical advantages, such as throwing spears or javelin (Rodríguez et al., 2016; Trinkaus, 1983; Trinkaus & Churchill, 1988). Curved bones have been argued to represent an optimum response to both internal (muscle and weight) and external loadings because of the effects of carrying, loading predictability, and more powerful rotational movements (Bertram & Biewener, 1988; Frost, 1973; Galtes et al., 2009; Lanyon, 1980; Yasutomi et al., 2002). Although the SH radial remains share general morphological patterns with Neanderthals, within the SH sample, there is some variation in the radial configuration; specimens with more anteriorly positioned radial tuberosity and shorter necks (Figure 21a and Figure 22f) tend to be less curved, while those that are more curved typically have longer necks (Figure 21) and more medially oriented radial tuberosity (Figure 22f).

It has been previously demonstrated that there is a bilateral asymmetry in the modern human humerus, Neanderthals, and SH humerus (Auerbach & Ruff, 2006; Carretero et al., 2023; Trinkaus et al., 1994). Rodríguez et al. (2016) determined that there are four SH individuals represented by paired complete radii: R-I and R-X, R-II and R-VI, R-IV and R-V, and R-VII and R-XI. Of these, one association (R-VII and R-XI) shows strong right-handed asymmetry, whereas a second association (R-II and R-VI) shows strong left-side asymmetry (Rodríguez et al., 2016). Thus, in this study, we detected probable left-handed hominins among adult SH

FIGURE 11 Ulna I, Right. Scale bar 5 cm. I interosseous, A anterior, M medial, P; posterior, R Radial, and Pr Proximal views.

FIGURE 12 Ulna VI, Left. Scale bar 5 cm. I interosseous, A anterior, M medial, P; posterior, R Radial, and Pr Proximal views.

FIGURE 13 Ulna VII Right. Scale bar 5 cm. I interosseous, A anterior, M medial, P posterior, R Radial, and Pr Proximal views.

individuals. This finding is in agreement with that of Carretero et al. (2023), who found an individual who was likely left-handed.

As mentioned above, the SH ulna remains had a high and massive olecranon process (Figure 25a), which was square-shaped when observed in the proximal view (Figure 24l). As can be seen in Table 8, a narrow olecranon process is a primitive trait shared by non-hominin apes, *Australopithecus*, *Homo ergaster*, and *Homo sapiens* (Aiello et al., 1999); therefore SH hominins have a derived trait compared with Neanderthals (Arsuaga et al., 2015; Boule, 1911; Trinkaus, 1983). SH ulnae have an anterior orientation of the trochlear notch (Figure 24k) which was considered a primitive trait by Churchill et al. (1996) and also being present in *Homo ergaster* (Solan & Day, 1992) as well as in the Klasies River Mouth fossil (Churchill et al., 1996), and shared with *Australopithecus* and *Homo ergaster*, along with Neanderthals (Pérez-Criado & Rosas, 2017).

Pérez-Criado and Rosas (2017) noted that most ulnar traits in Neanderthals have a primitive configuration, with the exception of the olecranon process. In this sense,

FIGURE 14 Ulna VIII, Left. Scale bar 5 cm. I interosseous, A anterior, M medial, P; posterior, R Radial, and Pr Proximal views.

SH ulnar remains are similar to Neanderthals in all their traits, except for the robusticity index, in which SH ulnae are more gracile than both modern humans and Neanderthals (Arsuaga et al., 2015).

The ulna is a fundamental component of the elbow joint and plays a key role in flexion and extension. Additionally, it can be considered a fixed part in forearm (radial) rotational movements; thus, it is also important in pronation-supination (Kapandji, 1999). The ulna articulates with the olecranon fossa of the distal humerus through the trochlear notch, which faces anteroproximally in *Homo sapiens*, but faces anteriorly in SH specimens, Neanderthals, and other archaic hominins (*H. ergaster*; *H. erectus*, Table 8). Therefore, the anterior orientation is an apomorphic trait of hominins. In contrast, in hominoids, the trochlear notch is more anteroproximally oriented, which is a plesiomorphic trait shared by the Omo L40-19 ulna (*Paranthropus aethiopicus*, Aiello et al., 1999) and modern humans. Trinkaus and Churchill (1988) stated that this morphology is not related to movement ranges, but rather to the loading

FIGURE 15 Ulna IX, Left. Scale bar 5 cm. I interosseous, A anterior, M medial, P posterior, R Radial, and Pr Proximal views.

FIGURE 16 Ulna X, Right. Scale bar 5 cm. I interosseous, A anterior, M medial, P posterior, R Radial, and Pr Proximal views.

FIGURE 17 Ulna XII, Right. Scale bar 5 cm. I interosseous, A anterior, M medial, P posterior, R Radial, and Pr Proximal views.

FIGURE 18 Ulna XIII, Left. Scale bar 5 cm. I interosseous, A anterior, M medial, P posterior, R Radial, and Pr Proximal views.

position, providing higher resistance to reaction forces in the joint.

Massive olecranon processes are typically observed in Neanderthals (Boule, 1911; Heim, 1982; Trinkaus, 1983). This trait, which is not observed in other hominis such as OH-36 (Aiello et al., 1999), is present in SH ulnae. A large olecranon process indicates a large insertion area for *m. triceps brachii*, but the position relative to the bone length is also important, as muscle insertion is located farther from the fulcrum compared to that of modern humans, favoring the lever arm of *m triceps brachii* of the elbow for extension (Trinkaus, 1983). The mean SH olecranon height was statistically similar to that in Neanderthals (Table 6). Thus, they share the highest position with the Neanderthals.

The *m. flexor digitorum superficialis* originates from the medial edge of the coronoid process, which is an important muscle for closing the hand. On the ulnar tuberosity, inserts *m. brachialis*, which flexes its elbow. Aiello and Dean (1990) concluded that a larger distance from the ulnar tuberosity to the olecranon (fulcrum) relative to the bone length, resulted in a more powerful lever arm for *m. brachialis*, favoring the flexion of the forear*m*.

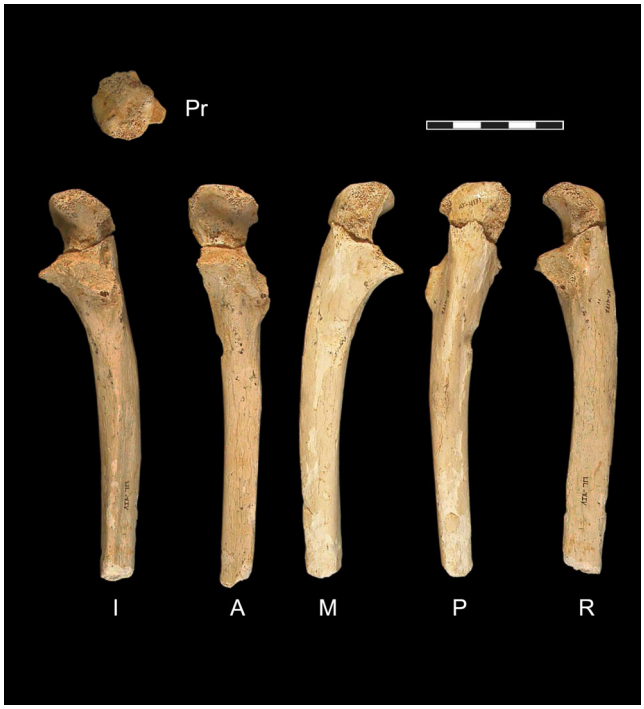

FIGURE 19 Ulna XIV, Left, Scale bar 5 cm, I interosseous, A anterior, M medial, P posterior, R Radial, and Pr Proximal views.

In the SH sample, the ulnar tuberosity is located more distally, with a longer distance between most proximal olecranon point to the distal point of the ulnar tuberosity (Ulnar tuberosity location index: Ulnar tuberosity length / maximum length = 26.5 ± 1.1, $n = 3$) than in modern humans (23.3 ± 1.3, $n = 28$). It was also located in a more medial position on the diaphysis (Figure 26). In addition, *m. brachialis* assists *m. biceps brachii* in flexing the forearm. The insertion of *m. biceps brachii* in the SH radii is located more distally and medially than in modern humans (Rodríguez et al., 2016) and is similar to that of Neanderthals, which favors supination and flexion movement (Trinkaus & Churchill, 1988).

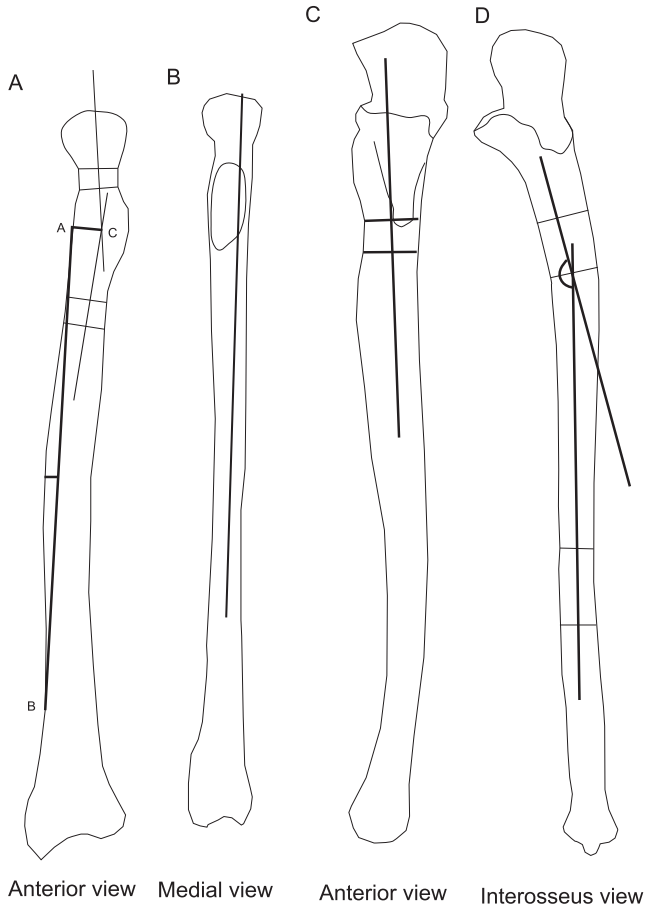

FIGURE 20 Radial and Ulnae special measurements. A Radial curvature, B radial tuberosity location. C ulnar tuberosity location and D ulnae curvature (see text for detailed explanations).

In humans, the supinator crest is long and courses from the end of the radial notch to the interosseous crest. The supinator muscles move the limb into the supination. The SH supinator crest is shorter and blunt compared to that of modern humans, and projects slightly (Figure 25f), resembling the conditions in Neanderthals (Boule, 1911; Heim, 1982; Trinkaus, 1983). The more lateral and projected positions of the supinator crest separate the axis of rotation from the point of force application, increasing the lever arm for rotation in fossil hominins. Furthermore, this causes the radial facet to be positioned differently from that in modern humans, with a more lateral, oblique, and sloped orientation relative to the ulnar diaphysis (Figure 25g). This location is also the insertion point of the radial collateral ligament, which stabilizes the elbow joint along with the ulnar collateral ligament.

The radial notch of the ulna of the SH specimens differed from that of modern humans in different orientations. The facet has a larger horizontal edge in modern humans, while it is more anteroposteriorly sloped in the SH due to the projection of the supinator crest mentioned above (Figure 25g). The posterior aspect projects slightly laterally compared to that of modern humans, in whom the facet is flatter and follows the shape of the diaphysis.

TABLE 7 Radial traits presence in hominins and other apes in comparison to Sima de los Huesos (SH) hominins.

Trait	Non-hominin Apes	*A. afarensis* *A. africanus*	*A. sediba*	*H. naledi*	Early *Homo*	*H. antecessor*	Neanderthals	SH
Head shape	AP > ML						AP > ML	AP > ML
Neck length	Long	Long	Short	Long	Long	Long	Long	Variable
Neck length index	Long	Long	Short	Long	Long	Long	Variable-long	Variable-long
Tuberosity orientation	Medial	Medial	Medial	Medial	Medial	Anterior	variable > medial	Variable > anterior
Curvature	Curved	Straight	Curved	Straight	Straight?	Straight	Curved	Curved
Robusticity	Robust	Robust	Robust	Robust	Robust	Gracile	Variable-Robust	Variable-Gracile
Distal epiphysis proportions							ML elongated	ML elongated

FIGURE 21 Sima de los Huesos (SH) radial trait description in anterior view A, Long neck. B, Neck angle less than 180. C, High Curvature. D, Less developmental of the interosseous crest. E, Small styloid process.

FIGURE 22 Sima de los Huesos (SH) radial trait description in medial view F Radial tuberosity, black line is the interosseous crest line.

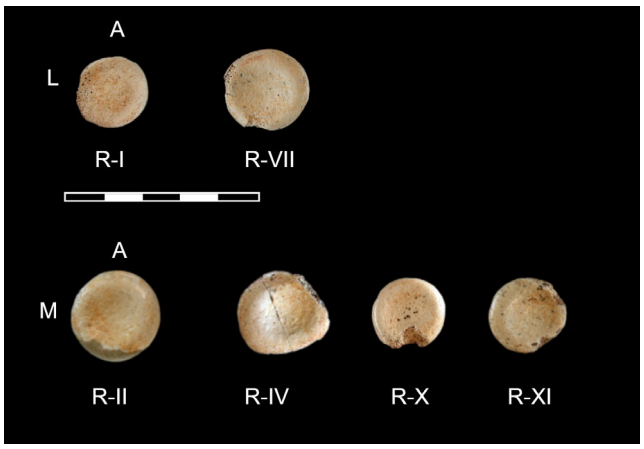

FIGURE 23 Sima de los Huesos (SH) radial sample in proximal view.

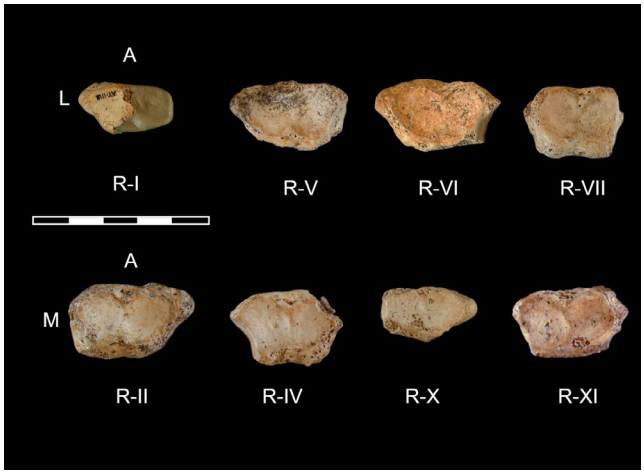

FIGURE 24 Sima de los Huesos (SH) radial sample in distal view compressed anteroposterior distal articulation.

This configuration moves the radial head anteriorly and proximally during rotation and brings the distal radius anteriorly, thereby increasing the lever arm for pronation.

Beneath the medial border of the coronoid process of the ulna, there is a ridge from which the two muscles partially originate; in the most proximal location, it is the

TABLE 8 Ulnar traits presence in hominins and other apes in comparison to Sima de los Huesos (SH).

Trait	Non-hominin Apes	*A. afarensis*	*A. africanus STW-431*	*Paranthropus OH-36*	*A. sediba*	*H. ergaster /erectus*	*Neanderthals*	SH
Olecranon shape	Narrow			Narrow		Narrow and rounded	Broad	Broad
Olecranon height	High	High	High	High	High	Low	High	High
Olecranon symmetry	Asymmetric	Symmetric	Asymmetric	Asymmetric	Asymmetric	Asymmetry	Symmetry	Symmetry
Trochlear notch orientation	Anteroproximal	Anterior		Anteroproximal	Anterior	Anterior	Anterior	Anterior
Trochlear notch longitudinal keel		Yes	Yes	Yes	Yes	Yes	No	No
Trochlear articulation		Wide	Narrow	Narrow	Narrow	Narrow	Wide	Wide
Trochlear articular surface orientation		Angulated	Angulated	Angulated	Angulated	Angulated	Same plane	Same plane
Radial notch shape		Semicircular		Teardrop	Teardrop	Shallow	Vertical	Vertical
Radial notch orientation	Anterior	Lateral	Lateral	Lateral	Lateral	Lateral	Lateral	Lateral
Supinator crest	Strongly developed	Strongly developed	Developed	Strongly developed	Developed	Strongly developed	Short and Blunt	Short and Blunt
Pronator teres crest				Developed	Soft	Rounded	Long	Long
Interosseous crest				Weakly developed	Weakly developed	Marked	Blunt	Blunt
Robusticity		Robust	Robust		Medium	Gracile	Robust	Gracile
Diaphysis Curve	AP curved	Moderately curved?	Straight	Curved	Straight	Straight	Curved ML and AP	Curved ML and AP

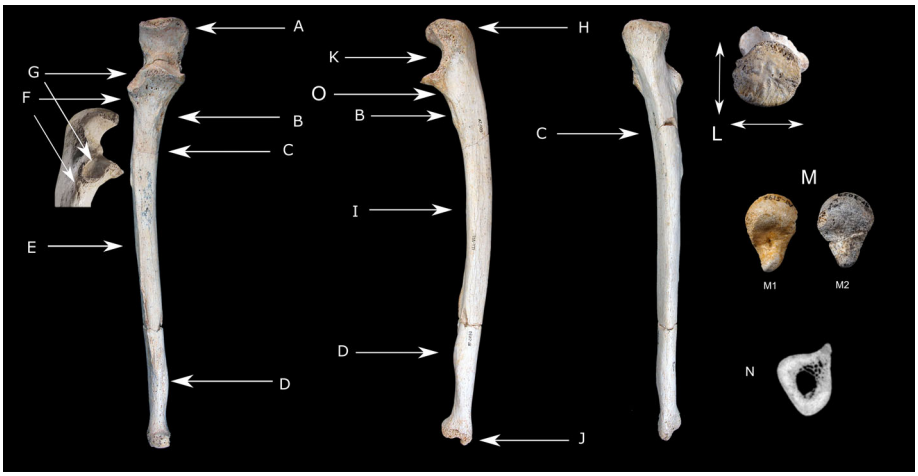

FIGURE 25 Sima de los Huesos (SH) ulnae trait definition A, *High and Massive olecranon process*; B, *M. brachialis* insertion; C, High mediolateral curvature in anterior and interosseous view; D, *M. pronator quadratus* insertion; E, weak interosseous crest; F, Rounded and developed supinator crest; G, Radial facet; H, Olecranon displaced anteriorly; K, Olecranon notch anteriorly oriented; I, Anteroposterior curvature in mediolateral view; J, Small styloid process; L, squared olecranon shape in proximal view; M, Ulna head; M1, relatively narrow; M2, relatively wide; N, Thick cortices; O, supinator crest.

FIGURE 26 M. *brachialis* location in Sima de los Huesos (SH) ulnae (a) and modern humans (b). Scale bar 5 cm.

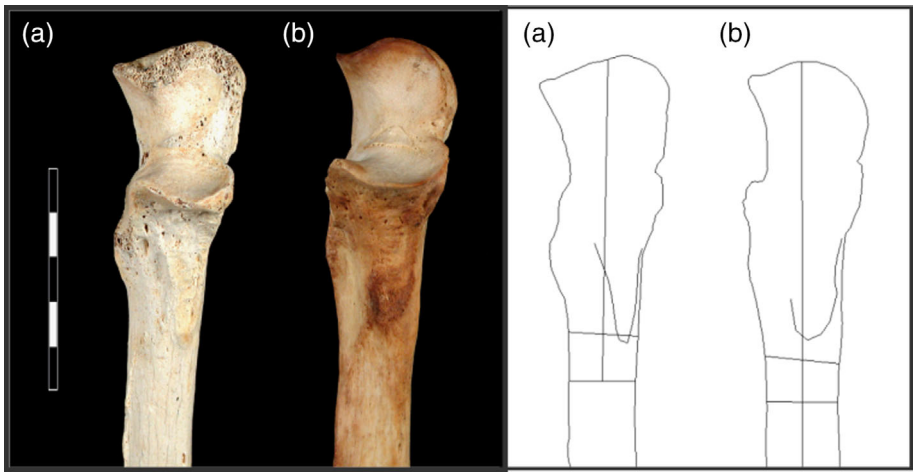

origin of *m. pronator teres* and distal to the origin of *m. flexor digitorum superficialis* (Stone & Stone, 1999). In SH individuals, this ridge is very pronounced, shorter than that in modern humans, and slightly displaced medially due to the most medially displaced *m. brachialis* (Figure 25o). In the case of *m. pronator teres*, as an assistant in flexion of the elbow joint, this position favors flexion because the ulna does not significantly move during pronation. This morphology is also common among Neanderthals and indicates greater development of the pronator teres.

In contrast to modern humans, where the *m. supinator* originates from a bony crest on the lateral border of the coronoid, in SH ulnar specimens it originates from a pronounced bony protrusion (Figure 25f). This protrusion separates and elevates the radial head in the radial notch of the proximal ulna, creating an axis of rotation (ulnar diaphysis) distinct from the muscular insertion in the radial diaphysis, which enables rotational movement. Additionally, owing to the curved shape of the radius, it can provide more efficient leverage for supination movements compared with modern humans.

Finally, SH ulnae have a relatively slender and laterally curved shaft (Figure 25c); traits they share with Neanderthals. Curved bones have been suggested as an optimal adaptation to internal loads, such as muscle and weight, as well as external loads. This is due to the carrying effect (Bertram & Biewener, 1988; Lanyon, 1980). Frost (1973) demonstrated that both morphological and experimental evidence support the idea that the curvature of long bones improves the predictability of loading. Additionally, a higher degree of diaphyseal curvature may result in more powerful rotational movements, because the entire mass of the forearm bone is situated

further from the axis of rotation (Galtes et al., 2009; Yasutomi et al., 2002). In the SH ulnar sample, there were only three ulnas that exceed 170° in curvature: UL-XII (172°), UL-VI (173°), and UL X (171°). These specimens can be included within the lower limits of the modern human range. Thus, the mean for the SH ulnae showed that they were more curved than those of modern humans. The curvature resembles that of Neanderthals (Figure 27).

It is generally accepted that Neanderthals have shorter distal limb segments (e.g., radius) than modern humans relative to their humeral length, and thus a lower brachial index (but see Holliday, 1997). This lower brachial index is typically described as a Neanderthal apomorphy and has been explained as an adaptation to avoid heat loss and, thus, leads to cold adaptation (Holliday, 1997; Trinkaus, 1981; Weaver, 2009). At the SH site, there is currently no clear evidence of a complete bony association of the entire upper limb, in a single individual. Therefore, we can deduce that the radii of the SH specimens were relatively longer than those of the Neanderthals. It is still uncertain whether this difference is due to climatic adaptation, but the general morphology of the SH forearm bone is more variable than that of the Neanderthals; therefore, in our view, genetic drift is a plausible explanation for the variation in Neanderthal body shape, as suggested by Weaver (2009). Moreover, it is important to note that the climate during the aforementioned period was warmer than that during the Neanderthal era and was similar to the present-day climate at the Sierra de Atapuerca sites, as demonstrated by Blain et al. (2009). Additional evidence is required for a more comprehensive understanding of this phenomenon.

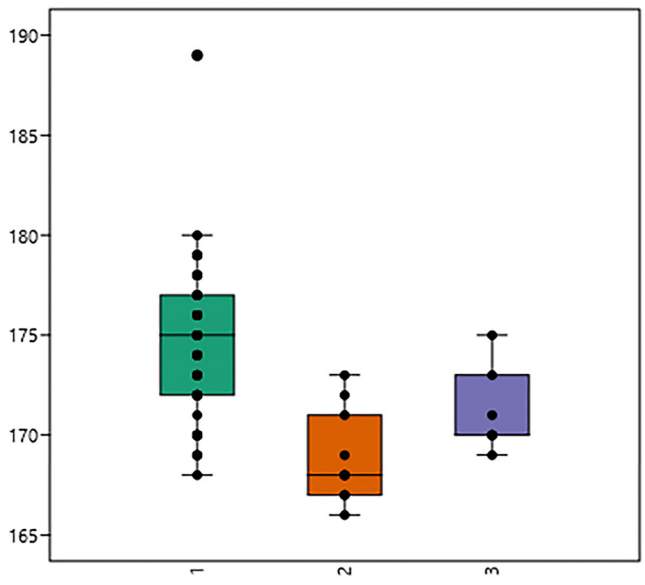

FIGURE 27 Ulna lateral curvature in degrees (y-axis). (1) Modern human sample in green, (2) orange Sima de los Huesos sample, and (3) purple Neanderthal sample.

5 | CONCLUSIONS

The recovery of radial and ulnar remains from the Atapuerca (SH) site, extended the known range of variation in some traits and confirmed previous observations regarding the differences and similarities between SH hominins and Neanderthals. The forearm bones of the SH specimens already show a Neanderthal morphological pattern, as has been described for the rest of the upper limb skeleton (Arsuaga et al., 2015; Carretero et al., 2023; García-González et al., 2023). The radii of the SH Site were similar to those of the Neanderthals in most of their derived traits, except for the robusticity index, in which the SH was more gracile than the Neanderthals. Additionally, the radial curvature, neck length, and orientation of the radial tuberosity of the SH radii were more variable, with some showing a clear Neanderthal-like pattern.

The ulnae of SH specimens were similar to the derived shape of Neanderthals, with a massive and high olecranon, gracile and curved bones, an anteriorly oriented trochlear notch, a proximal radial notch with a rhomboidal shape, a blunt and elevated supinator crest, and the insertion of *m*. brachialis located distally and medially.

Overall, the SH forearm had curved ulna and radius bones that increased the distance between the origin and the insertion of the *m. pronator quadratus* and origin, and the insertion of *m. pronator teres*, increasing the distance from the axis of pronation and supination (ulna) to the radius, thus moving the radial mass further from the axis of rotation and favoring pronation-supination movement. The more developed and laterally projected supinator crest in the ulnae, along with the location and shape of the radial notch, facilitates this movement. Moreover, the radial tuberosity of *m. biceps brachii* is located medially to the interosseous crest, which improves the maintenance of strength through the full range of pronation and supination without losing power during the final phases of supination, as in Neanderthals (Aiello & Dean, 1990; Pearson & Grine, 1997; Trinkaus & Churchill, 1988). The ulnar tuberosity is also located medially to the elbow and in a more distal position than that in modern humans, converting *m*. brachialis into a more efficient flexor, assisting the *m*. biceps brachii.

However, the SH ulnae have a pronounced posterior subtension and a more anterior-facing trochlear notch, providing greater resistance to joint reaction forces in

partial flexion of the elbow, suggesting different habitual behavior, resulting in frequency differences in the habitual position of peak loading, as observed in Neanderthals by Trinkaus and Churchill (1988).

Finally, the morphology of the forearm bones in individuals from SH was similar to that of Neanderthals, but with variations in the frequency of the appearance of some of these traits, with SH showing greater variation than Neanderthals. This may indicate that, in our view, the overall morphology of Neanderthals is more likely a result of a genetic drift, where Neanderthals retain only certain traits that are already present in humans from the SH, rather than being solely an adaptation to the cold climate, as already pointed out by Weaver (2009), Holton and Franciscus (2008), Rae et al. (2011), Balzeau et al. (2023), and Li et al. (2023).

AUTHOR CONTRIBUTIONS

Laura Rodríguez: Conceptualization; investigation; writing – original draft; methodology; writing – review and editing; formal analysis. **Rebeca García-González:** Conceptualization; investigation; writing – review and editing; formal analysis; methodology; writing – original draft. **Juan Luis Arsuaga:** Funding acquisition; conceptualization; supervision; project administration. **José-Miguel Carretero:** Conceptualization; formal analysis; investigation; writing – review and editing; methodology.

ACKNOWLEDGMENTS

- We benefited from fruitful discussions with our colleagues from the Centro UCM-ISCIII Sobre Evolución y Comportamiento Humanos of Madrid and the Laboratorio de Evolución Humana, at the University of Burgos.
- Thanks to the anonymous reviewers of the manuscript for their valuable comments.
- We thank our companions in the Atapuerca research and the SH excavation team for their invaluable dedication to the ongoing work at the SH site.
- Thanks to Maria Cruz Ortega for her extraordinary and patient restoration of the fossils.
- We acknowledge Javier Trueba for the extraordinary graphic documentation of the SH fossils and fieldwork under demanding conditions.
- The following individuals and their institutions had access to modern and fossil comparative materials: P. Mennecier and A. Froment (Muséum National dHistoire Naturelle), Y. Haile-Selassie, B. Latimer, L. Jellema (Cleveland University of Natural History), E. Cunha and A. L. Santos (Coimbra University), A. Marcal (Bocage Museum), and T. Holliday (Tulane University).
- The fossil analyzed in this work are from the "Colección Museística de Castilla y León" of the Junta de Castilla y León.

FUNDING INFORMATION

- The Atapuerca Research Project was financed by MCIN/AEI/10.13039/501100011033/FEDER, UE, grant number PID2021-122355NB-C31.
- Fieldwork at the Atapuerca sites is funded by the Junta de Castilla y León and the Fundación Atapuerca.

CONFLICT OF INTEREST STATEMENT

The authors declare no conflicts of interest.

ORCID

Laura Rodríguez https://orcid.org/0000-0002-5090-1582
Rebeca García-González https://orcid.org/0000-0002-1035-6655
José-Miguel Carretero https://orcid.org/0000-0003-0409-8087

REFERENCES

Aiello, L. C., & Dean, C. (1990). *An Introduction to Human Evolutionary Anatomy*. Academic Press Limited.

Aiello, L. C., Wood, B., Key, C., & Lewis, M. (1999). Morphological and taxonomic affinities of the Olduvai ulna (OH 36). *American Journal of Physical Anthropology*, *109*(1), 89–110.

Antón, S. C., & Polidoro, G. M. (2000). Prehistoric radio-ulnar synostosis: Implicarions for function. *International Journal of Osteoarchaeology*, *10*, 189–197.

Arsuaga, J. L., Carretero, J.-M., Lorenzo, C., Gómez-Olivencia, A., Pablos, A., Rodríguez, L., García-González, R., Bonmatí, A., Quam, R. M., Pantoja-Pérez, A., Martínez, I., Aranburu, A., Gracia-Téllez, A., Poza-Rey, E., Sala, N., García, N., Alcázar de Velasco, A., Cuenca-Bescós, G., Bermúdez de Castro, J. M., & Carbonell, E. (2015). Postcranial morphology of the middle Pleistocene humans from Sima de los Huesos, Spain. *Proceedings of the National Academy of Sciences*, *112*(37), 11524.

Auerbach, B. M., & Ruff, C. B. (2006). Limb bone bilateral asymmetry variability and commonality among modern humans. *Journal of Human Evolution*, *50*, 203–218.

Balzeau, A., Albessard-Ball, L., Kubicka, A. M., Filippo, A., Beaudet, A., Santos, E., Bienvenu, T., Arsuaga, J.-L., Bartsiokas, A., Berger, L., Bermúdez de Castro, J. M., Brunet, M., Carlson, K. J., Daura, J., Gorgoulis, V. G., Grine, F. E., Harvati, K., Hawks, J., Herries, A., … Buck, L. T. (2023). Frontal sinuses and human evolution. Science. *Advances*, *8*(42), eabp9767.

Bar Yosef, O., & Vandermeersch, B. (1991). Le squelette moustérien de Kébara 2. Ed. CNRS, 25(5), p.584, 1992.

Bertram, J. E. A., & Biewener, A. A. (1988). Bone curvature: Sacrificing strenght for load predictibility? *Journal of Theorical Biology*, *131*, 75–92.

Blain, H.-A., Bailon, S., Cuenca-Bescós, G., Arsuaga, J. L., Bermúdez de Castro, J. M., & Carbonell, E. (2009). Long-term climate record inferred from early-middle Pleistocene

amphibian and squamate reptile assemblages at the Gran Dolina Cave, Atapuerca, Spain. *Journal of Human Evolution*, *56*(1), 55–65.

Boule, M. (1911). L'Homme Fossile de La Chapelle aux Saints. Masson et C, Editeurs.

Buikstra, J., & Ubelaker, D. H. (1994). Standards for data collection from human skeletal remains.

Cardoso, H. F. (2006). Brief communication: The collection of identified human skeletons housed at the Bocage Museum (National Museum of Natural History), Lisbon, Portugal. *American Journal of Physical Anthropology: The Official Publication of the American Association of Physical Anthropologists*, *129*(2), 173–176.

Carretero, J. M. (1994). Estudio del esqueleto de las dos cinturas y el miembro superior de los homínidos de la Sima de los Huesos, Sierra de Atapuerca, Burgos. [Tesis Doctoral]. Universidad Complutense.

Carretero, J. M., García-González, R., Rodríguez, L., & Arsuaga, J. L. (2023). Main anatomical characteristics of the hominin fossil humeri from the Sima de los Huesos Middle Pleistocene site, Sierra de Atapuerca, Burgos, Spain: An update. The Anatomical Record, n/a(n/a).

Carretero, J. M., Lorenzo, C., & Arsuaga, J. L. (1999). Axial and appendicular skeleton of Homo antecessor. *Journal of Human Evolution*, *37*(3–4), 459–499.

Churchill, S. E., Pearson, O. M., Grine, F. E., Trinkaus, E., & Holliday, T. W. (1996). Morphological affinities of the proximal ulna from Klasies River main site: Archaic or modern? *Journal of Human Evolution*, *31*, 213–237.

Coqueugniot, H., & Weaver, T. D. (2007). Brief communication: Infracranial maturation in the skeletal collection from Coimbra, Portugal: New aging standards for epiphyseal union. *American Journal of Physical Anthropology*, *134*(3), 424–437.

De Groote, I. (2011). The Neanderthal lower arm. *Journal of Human Evolution*, *61*(4), 396–410.

Frost, H. M. (1973). *Orthopaedic Biomechanics*. Charles C Thomas.

Galtes, I., Jordana, X., Malgosa, A., & Manyosa, J. (2009). Technical note: Forearm pronation efficiency analysis in skeletal remains. *American Journal of Physical Anthropology*, *140*(3), 589–594.

García-González, R., Rodríguez, L., Salazar-Fernández, A., Arsuaga, J. L., & Carretero, J.-M. (2023). Updated study of adult and subadult pectoral girdle bones from Sima de los Huesos site (Sierra de Atapuerca, Burgos, Spain). Anatomical and age estimation keys. The Anatomical Record.

Heim, J. L. (1982). Les Hommes fossiles de la Ferrasie. Vol. Tome II: Squelette des membres. Masson.

Holliday, T. W. (1997). Postcranial evidence of cold adaptation in European Neandertals. *American Journal of Physical Anthropology*, *104*(2), 245–258.

Holton, N. E., & Franciscus, R. G. (2008). The paradox of a wide nasal aperture in cold-adapted Neandertals: A causal assessment. *Journal of Human Evolution*, *55*(6), 942–951. https://doi.org/10.1016/j.jhevol.2008.07.001

Kapandji, A. I. (1999). Fisiología articular: Miembro superior: Vol. I. Editorial medica panamericana.

Lanyon, L. E. (1980). The influence of function on the development of bone curvature. An experimental study on the rat tibia. *Journal of Zoology*, *192*(4), 457–466.

Li, Q., Chen, J., Faux, P., Delgado, M. E., Bonfante, B., Fuentes-Guajardo, M., Mendoza-Revilla, J., Chacón-Duque, J. C., Hurtado, M., Villegas, V., Granja, V., Jaramillo, C., Arias, W., Barquera, R., Everardo-Martínez, P., Sánchez-Quinto, M., Gómez-Valdés, J., Villamil-Ramírez, H., Silva de Cerqueira, C. C., … Ruiz-Linares, A. (2023). Automatic landmarking identifies new loci associated with face morphology and implicates Neanderthal introgression in human nasal shape. *Communications Biology*, *6*(1), 481. https://doi.org/10.1038/s42003-023-04838-7

Lorenzo, C. (2007). *Evolución de la mano en los homínidos. Análisis morfológico de los fósiles de la Sierra de Atapuerca [Tesis Doctoral]*. Universidad Complutense de Madrid.

Maia Nieto, M. A. (1957). Estudo osteometrico do antebraço nos portugueses. Universidad de Coimbra. Estudio osteométrico do antebraço nos portugueses. Contribuiçones para o Estudo da Antropologia Portuguesa VI (6), 141e222.

Martin, R., & Saller, K. (1957). Lehrbuch der Anthropologie. Vol. Band 1. Gustav Fischer Verlag.

McCown, T. D., & Keith, A. (1939). *The stone age of Mount Carmel II: The fossil human remains from the Levalloiso-Mousterian*. Clarendon Press.

McHenry, H. M., Corruccini, R. S., & Howell, F. C. (1976). Analysis of an early hoiminid ulna from the Omo Basin, Ethiopia. *American journal of physical anthropology*, *44*(2), 295–304.

Mednikova, M. B. (2013). An archaic human Ulna from Chagyrskaya Cave Altai: Morphology and Taxonomy*. *Archaeology, Ethnology and Anthropology of Eurasia*, *41*(1), 66–77.

Meulam, J. J., & Heiser, W. J. (2019). IBM SPSS Categories, 26.

Pearson, O. M., & Grine, F. E. (1997). Re-analysis of the hominid radii from Cave of Hearths and Klasies River Mouth, South Africa. *Journal of Human Evolution*, *32*(6), 557–592.

Pérez-Criado, L., & Rosas, A. (2017). Evolutionary anatomy of the Neandertal ulna and radius in the light of the new El Sidrón sample. *Journal of Human Evolution*, *106*, 38–53.

Phenice, T. W. (1969). A newly developed visual method of sexing the os pubis. *American Journal of Physical Anthropology*, *30*(2), 297–301.

Rae, T. C., Koppe, T., & Stringer, C. B. (2011). The Neanderthal face is not cold adapted. *Journal of Human Evolution*, *60*(2), 234–239.

Rodríguez, L., Carretero, J. M., García-González, R., Lorenzo, C., Gómez-Olivencia, A., Quam, R., Martínez, I., Gracia-Téllez, A., & Arsuaga, J. L. (2016). Fossil hominin radii from the Sima de los Huesos Middle Pleistocene site (Sierra de Atapuerca, Spain). *Journal of Human Evolution*, *90*, 55–73.

Senut, B. (1980). New data on the humerus and its joints in Plio-Pleistocene Hominids. *Collegium Antropologicum*, *4*(1), 87–93.

Solan, M., & Day, M. H. (1992). The Baringo (Kapthurin) ulna. *Journal of Human Evolution*, *22*, 307–313.

Stone, R. J., & Stone, J. (1999). *Atlas of skeletal muscles*. McGrawn Hill.

Trinkaus, E. (1981). Neanderthal limb proportions and cold adaptation. In C. Stringer (Ed.), *Aspects of Human Evolution*. Taylor and Francis.

Trinkaus, E. (1983). *The Shanidar Neandertals*. Academic Press.

Trinkaus, E., & Churchill, S. E. (1988). Neandertal radial tuberosity orientation. *American Journal of Physical Anthropology*, *75*(1), 15–21.

Trinkaus, E., Churchill, S. E., & Ruff, C. B. (1994). Postcranial Robusticity in Homo II. Humeral Bilateral Asymmetry and Bone Plasticity. *American Journal of Physical Anthropology*, *93*(1), 1–34.

Trinkaus, E., Churchill, S. E., Ruff, C. B., & Vandermeersch, B. (1999). Long Bone shaft robusticity and body proportions of the Saint-Césaire 1 Châtelperronian Neanderthal. *Journal of Archaeological Science*, *26*(7), 753–773.

Weaver, T. D. (2009). The meaning of Neandertal skeletal morphology. *Proceedings of the National Academy of Sciences*, *106*, 16028–16033.

Yasutomi, T., Nakatsuchi, Y., Kioke, H., & Uchiyama, S. (2002). Mechanisms of limitation of pronation/supination of the forearm in geometric models of deformities of the forearm bones. *Clinical biomechanics*, *17*, 456–463.

How to cite this article: Rodríguez, L., García-González, R., Arsuaga, J. L., & Carretero, J.-M. (2023). Uncovering the adult morphology of the forearm bones from the Sima de los Huesos Site in Atapuerca (Spain), with comments on biomechanical features. *The Anatomical Record*, 1–25. https://doi.org/10.1002/ar.25281